8th International Colloquium on Bluff Body Aerodynamics and Applications
Northeastern University, Boston, Massachusetts, USA
June 7 - 11, 2016

Vortex-shedding mechanism for the BARC rectangular section in smooth and turbulent flow

Claudio Mannini[a,*], Antonino Maria Marra[a], Luca Pigolotti[a], Gianni Bartoli[a]

[a]*CRIACIV/Department of Civil and Environmental Engineering, University of Florence, Italy,*
claudio.mannini@unifi.it, antoninomaria.marra@unifi.it, luca.pigolotti@dicea.unifi.it,
gianni.bartoli@unifi.it

SUMMARY:
The aerodynamic behavior of the rectangular 5:1 cylinder is the object of an international numerical and experimental benchmark study (BARC). In this work, the unsteady characteristics of the high-Reynolds number flow past the cylinder was studied in the wind tunnel; pressure measurements were performed on a sectional model in smooth and turbulent flows, while wake velocity measurements were carried out in smooth flow only. In particular, the paper is devoted to shed some light on the vortex shedding mechanism due to the impinging shear-layer instability in smooth and various turbulent flows.

Keywords: BARC, Rectangular Cylinder, Wind Tunnel Tests, Turbulent Flow, Impinging Shear-Layer Instability

1. INTRODUCTION

The rectangular shape is a recurring geometry in civil and industrial engineering practice and therefore it has often been the object of studies concerning its aerodynamic and aeroelastic behavior. For a theoretical cross section with perfectly sharp corners and smooth surfaces, only one parameter, namely the side ratio, defines the rectangular geometry. Due to its simplicity, it clearly highlights interesting fluid dynamic phenomena and allows a detailed study of the aerodynamic features of the generated flow field. Moreover, depending on the side ratio and turbulent characteristics of the incoming flow, rectangular prisms are prone to different types of flow-induced excitation, such as vortex-induced vibration, hard- and soft-type transverse galloping, interference of vortex-induced vibration and galloping, torsional galloping (or torsional flutter), coupled flutter [see *e.g.* (Mannini, Marra, et al., 2014; Marra et al., 2015; Matsumoto, 1996; Nakamura and Ohya, 1984; Naudascher and Wang, 1993; Parkinson, 1965; Shiraishi and Matsumoto, 1983; Washizu et al., 1978)]. Consequently, it is extremely important from the practical engineering point of view to highlight the main features of the flow past these simple geometries and to understand those mechanisms that can produce vibrations of elastic structures.

For all these reasons, the BARC benchmark was launched in 2008 during the 6th International Symposium on Bluff Body Aerodynamics and Applications (Bartoli et al., 2008), focusing on the stationary rectangular 5:1 cylinder, where the short side of the section faces the flow. This side ratio is particularly interesting, since in smooth flow the shear layers separating at the leading edges are known to reattach intermittently close to the trailing edges, so that a strong sensitivity of its aerodynamics on several geometrical features and flow conditions is expected. In addition, Ohya et al. (1992) noted that the vortex shedding mechanism is less regular (and then challenging to predict) than for slightly smaller (such as 3:1 and 4:1) or larger (such as 6:1) side ratios. A

synopsis of the experimental and numerical results obtained in the first four years of activity has been recently published (Bruno, Salvetti, et al., 2014).

For the BARC section, and in general for rectangular cylinders with side ratios in the range between 3 and 15, the vortex shedding mechanism is not of Kármán type, *i.e.* triggered directly by the interaction between upper and lower shear layers, but it is due to the "impinging shear layer instability" (Nakamura, Ohya, and Tsuruta, 1991; Ohya et al., 1992; Rockwell and Naudascher, 1979). This phenomenon is also known as "impinging leading-edge vortices" (Naudascher and Wang, 1993) and is produced by the "impinging" of a shear layer on an obstacle downstream, namely the afterbody in the trailing edge region in the case of rectangular cylinders. This generates a feedback control through pressure pulses that travel upstream at the speed of sound. This feedback may be an order of magnitude stronger than natural feedback in the absence of impingement and is able to trigger large flow fluctuations at the leading edge. In fact, Nakamura and Nakashima (1986) showed that shear layer instability, vortex shedding and vortex excitation are possible for rectangular, H and T shapes also in the presence of a splitter plate. Impinging shear layer instability exhibits different modes of vortex shedding depending on the side ratio, which in some cases can also coexist. As a consequence, the Strouhal number presents evident jumps in correspondence of the side ratios for which a switch to a higher vortex-shedding mode occurs. In addition, Hourigan et al. (2001), through direct numerical simulations, and Mills et al. (2002), through flow visualizations and PIV measurements, studied the interaction phenomena between leading- and trailing-edge vortices and their phasing in rectangular cylinders with significant afterbody.

This paper reports the results of wind tunnel measurements of unsteady surface pressures and wake flow velocities on a large stationary sectional model of particularly high quality. The effects of changing both the turbulence intensity and the integral length scale of the incoming flow were investigated, with particular attention to the mechanism of vortex shedding.

2. WIND TUNNEL TESTS

The tests were carried out in the open-circuit boundary-layer CRIACIV wind tunnel in Prato, Italy. The facility is about 22 m long, with a rectangular test section 2.42 m $\times$ 1.60 m. The flow speed can be varied continuously up to 30 m/s and, in the absence of turbulators, the free-stream turbulence intensity is around 0.7%. Homogeneous turbulent flows were generated by means of two different grids variably distanced upstream of the model. The obtained longitudinal turbulence intensity I_u was between 2.9% and 13.6%, while the integral length scale L_{ux}/D was in the range 0.6 to 4.4,

Table 1. Turbulent flow characteristics of the tests performed. Δx denotes the distance between the grid and the longitudinal axis of the model, I_u the turbulence intensity and L_{ux} the longitudinal turbulence integral length scale

Configuration	Grid	Δx [m]	I_u [%]	L_{ux}/D [-]
#1	no grid	-	0.7	-
#2	A	4.95	2.9	1.3
#3	A	1.50	5.7	0.7
#4	A	0.90	8.6	0.6
#5	B	7.14	8.8	4.4
#6	B	4.95	13.6	3.9

(a) (b)

Figure 1. View of the model (a); model in the wind tunnel (b)

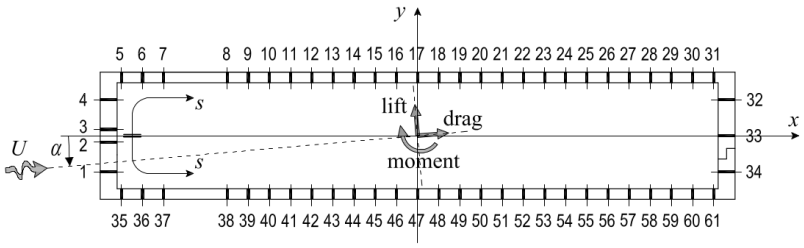

Figure 2. Distribution of the pressure taps along the cross section, with representation of the convention for the reference coordinates, the angle of attack and the aerodynamic forces

where D is the cross-wind section dimension of the cylinder (Table 1).

The model was made of a special aluminum alloy, with very sharp edges and smooth surfaces (Figure 1(a)). It was 300 mm wide (B), 60 mm deep (D) and 2380 mm long (L). It was mounted horizontally in the wind tunnel, with its longitudinal axis perpendicular to the flow stream (Figure 1(b)). Even if its ends were positioned very close to the wind-tunnel lateral walls, end-plates were also provided to avoid base pressure increase in the lateral regions of the model. The blockage ratio was 3.75% at zero degree angle of attack and 6.95% at the maximum angle of attack tested ($\alpha = \pm 10°$). The Reynolds number, referred to the section depth D, was in the range $12,000 \leq Re \leq 117,000$.

The model was provided with 564 pressure taps and 61 of them, selected in the midspan section (Figure 2), were connected to miniaturized piezoelectric scanners, sampling at a rate of 500 Hz. The measurement of the aerodynamic force coefficients at various angles of attack were performed by means of two high-frequency six-components strain-gauges dynamometers. Finally, the characteristics of the smooth or turbulent oncoming flows and the longitudinal velocity fluctuations in the wake of the cylinder were measured through a single-component hot-wire anemometer.

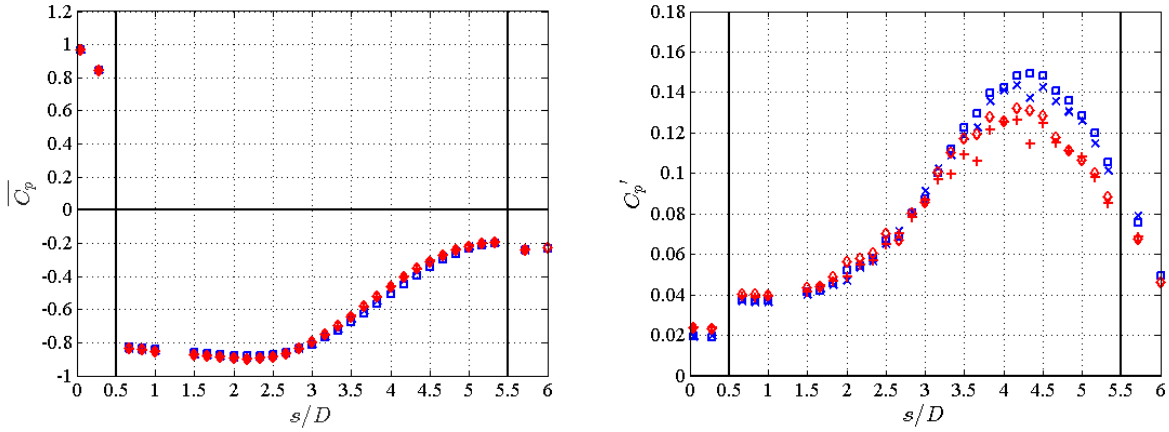

(a) (b)

Figure 3. Mean and standard deviation of pressure coefficients in smooth flow for $\alpha = 0°$ and three values of the Reynolds number. $s/D = 0$ and $s/D = 6$ denote respectively the windward- and leeward-face midpoint of the model

3. RESULTS IN SMOOTH FLOW

Prior to starting the tests, the exact position of zero angle of attack was sought by comparing the pressure distributions on the upper and lower side of the instrumented section of the cylinder and it was obtained by rotating nose-up the model of 0.45°. The Reynolds number $Re = U_\infty D/\nu$, being U_∞ the undisturbed flow speed and ν the air kinematic viscosity, was varied up to 112,200 and its effect on the mean pressure coefficient distribution was found to be very small, as shown in Figure 3. By contrast, small but non-negligible differences can be noticed in the standard deviation of pressure fluctuations.

The Strouhal number $St = n_s D/U_\infty$, n_s being the frequency of vortex shedding, was determined from the analysis of the pressure-taps time histories, detecting the frequency corresponding to the dominant peak in the spectra. It resulted to be about 0.115, which is coherent with the literature results collected in Mannini et al. (2011). Nevertheless, the inspection of the pressure power spectral density for all the pressure taps, revealed other interesting features. It can be noticed that the great majority of the energy of pressure fluctuations is provided by the Strouhal peak. However, slightly moving downstream from the leading edges, the total variance remains approximately unchanged in a first portion of the lateral sides of the cylinder ($0.5 \leq s/D \lesssim 2$, see Figure 3(b)) but the vortex-shedding peak progressively reduces, due to the enhancement of the background component of the fluctuations. Prior to reaching the midchord, for instance at $s/D = 2.5$, where the total variance has just started to increase, the spectrum is broad-banded and the Strouhal peak is hardly detectable. Going further downstream, the Strouhal peak becomes dominant again, particularly in the region of the maximum of the standard deviation. Then, approaching the trailing edge, the magnitude of the peak around $nD/U = 0.115$ tends to decrease.

Measurements with a hot-wire anemometer in the wake of the model were performed for $\alpha = 0°$ in smooth flow along a transversal line at a distance equal to $2D$ downstream of the rear face of the model (Figure 4). Some results are reported in Figure 5, where y denotes the distance from the wake centerline. The local mean flow velocity U is very low near the wake centerline and it quickly

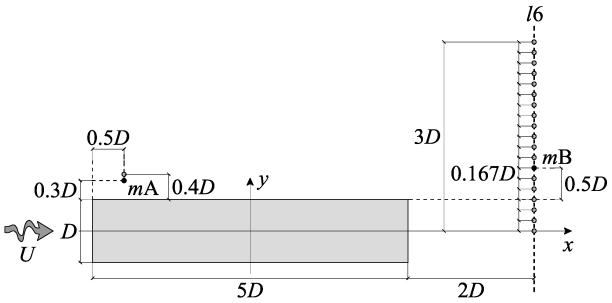

Figure 4. Position of the anemometry measurement points in the wake of the cylinder; $l6$, mA and mB represent respectively a reference transverse line and two reference points of the benchmark study (Bartoli et al., 2008)

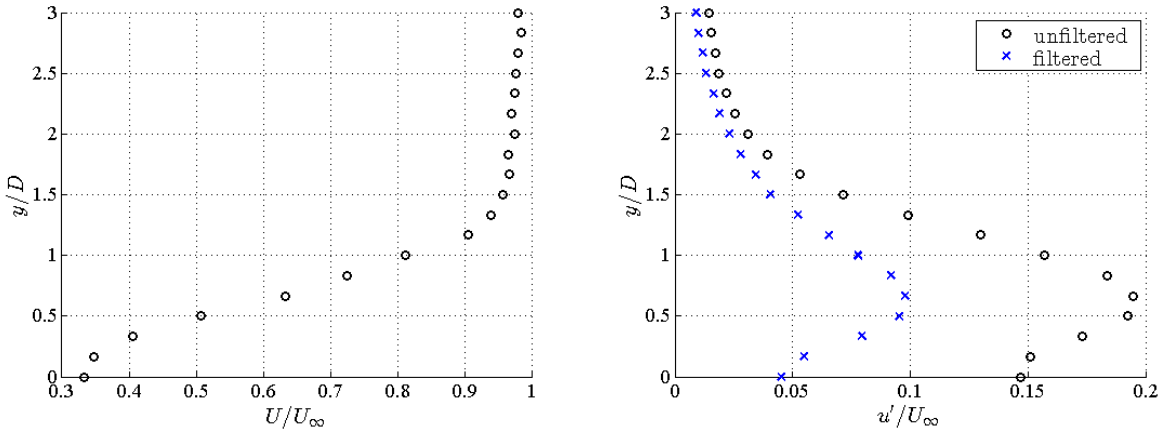

Figure 5. Statistical moments of streamwise velocity fluctuations $u(t)$ along the transverse line $l6$, located at a distance equal to $2D$ downstream the rear face of the model (Figure 4). $y/D = 0$ denotes the wake centerline, while $y/D = 1$ corresponds to the point mB. The Reynolds number is 112,600.

increases with the transverse distance in the range $0.3 \lesssim y/D \lesssim 1.5$. For $y/D \cong 1.5$ the velocity recovery is nearly complete. By contrast, the standard deviation u' of the velocity fluctuations reaches a maximum for $y/D \cong 0.65$ and then rapidly decreases. It is known that the point of maximum velocity fluctuation coincides with the location of the vortex centers. Furthermore, the velocity fluctuation time histories were processed with a bandpass filter around the Strouhal frequency and the results are shown in Figure 5 together with the statistics of the unfiltered signals.

4. RESULTS IN TURBULENT FLOW

The effect of turbulence on the pressure coefficient distributions is shown in Figure 6. It is apparent that even a small turbulence intensity is able to significantly reduce the length of the recirculation bubbles on the lateral faces of the model, as shown by the faster recovery of mean pressures and the upstream shift of the standard-deviation peak, which is known to be related to the location of the mean reattachment point. Higher turbulence intensities produce a more pronounced shortening of the side bubble length. In addition, given the same turbulence intensity, a value of L_{ux}/D of 4.4 instead of 0.6 entails longer bubbles and, due to the enhanced correlation of the incoming flow, higher pressure fluctuation values, in particular in the first half of the lateral side of the cylinder.

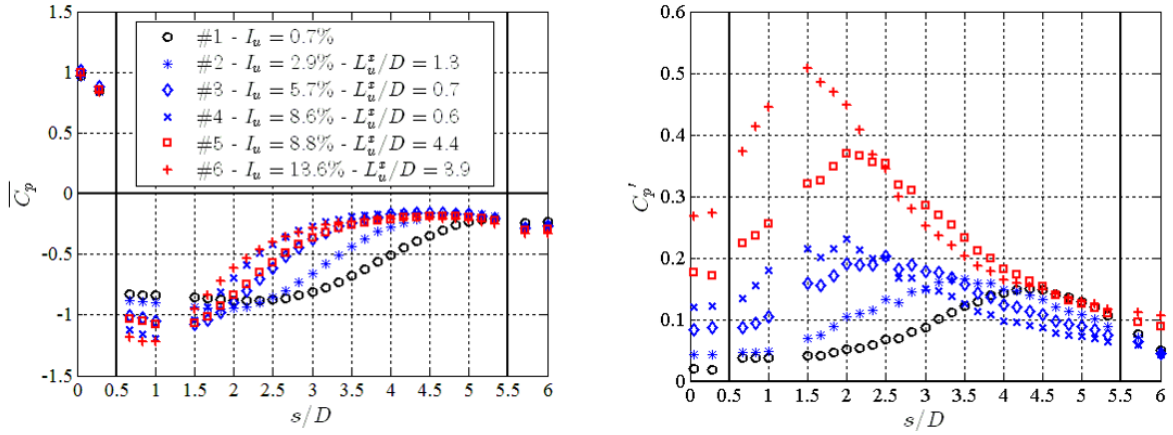

(a) (b)

Figure 6. Mean (a) and standard deviation (b) of pressure coefficients ($\alpha = 0°$, $55,900 \leq Re \leq 60,000$) in smooth and various turbulent flows.

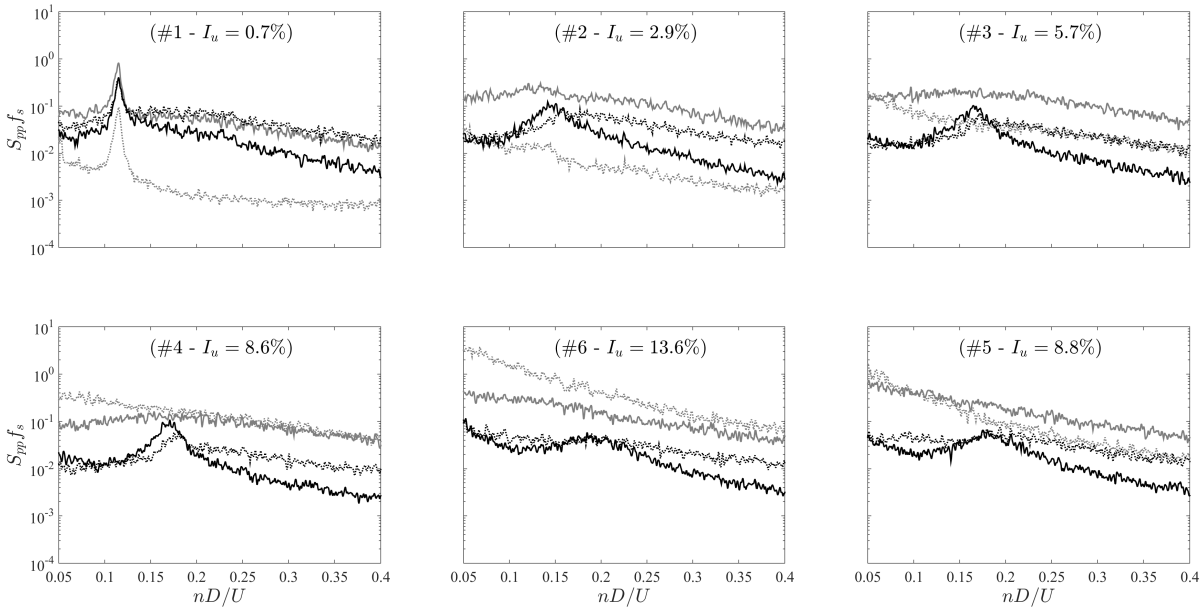

Figure 7. Dimensionless power spectral density of the pressure coefficient for tap 37, at $s/D = 1.0$ (grey-dotted), tap 49, at $s/D = 3.3$ (grey-solid), tap 60, at $s/D = 5.3$, (black-dotted), and tap 34 at $s/D = 5.7$, (black-solid), for zero angle of attack and various turbulence conditions ($55,900 \leq Re \leq 60,000$).

As shown in Figure 7, in turbulent flow no sharp peaks appear in the pressure power spectral density and for some pressure taps the energy contribution at the vortex-shedding frequency is masked by the background of the spectra. The Strouhal peak is more evident near the trailing edges and in the base region.

Figure 8 was built by examining the pressure spectra of all the pressure taps and identifying the

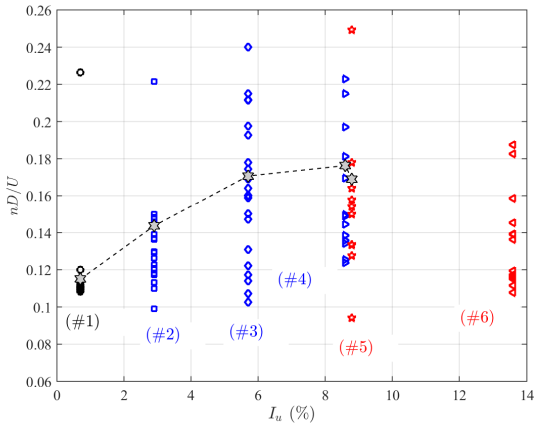

Figure 8. Values of the dominant peak in the spectra of pressure coefficients with respect to turbulence conditions for all the pressure taps ($55,900 \leq Re \leq 60,000$). The dashed line highlights the values of the Strouhal number determined from the lift coefficient spectra.

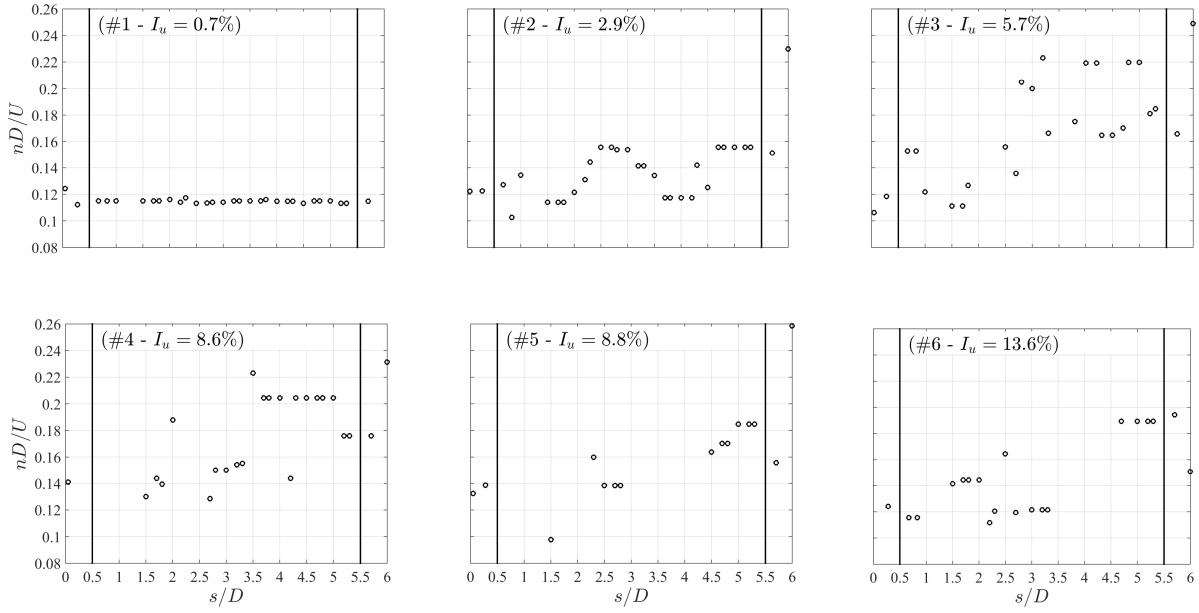

Figure 9. Dimensionless frequency corresponding to the dominant peak in the power spectral density of the pressure taps along the contour of the section in smooth and various turbulent flows ($55,900 \leq Re \leq 60,000$).

highest peak, if any. In smooth flow, the peaks occur all in the same range, with the exception of the base region where the dominant frequency in the spectra is that corresponding to $2St$. By contrast, peaks in the whole range of dimensionless frequencies between about 0.1 to about 0.24 can be observed in turbulent flow. However, it is worth noting that generally this effect is not due to spectral irregularities but to the presence of several peaks that in turn become dominant in different locations of the section contour. Figure 9 and Figure 10 better underscore this behavior. For the pressure taps with no value reported in Figure 9, no evident peak was detectable.

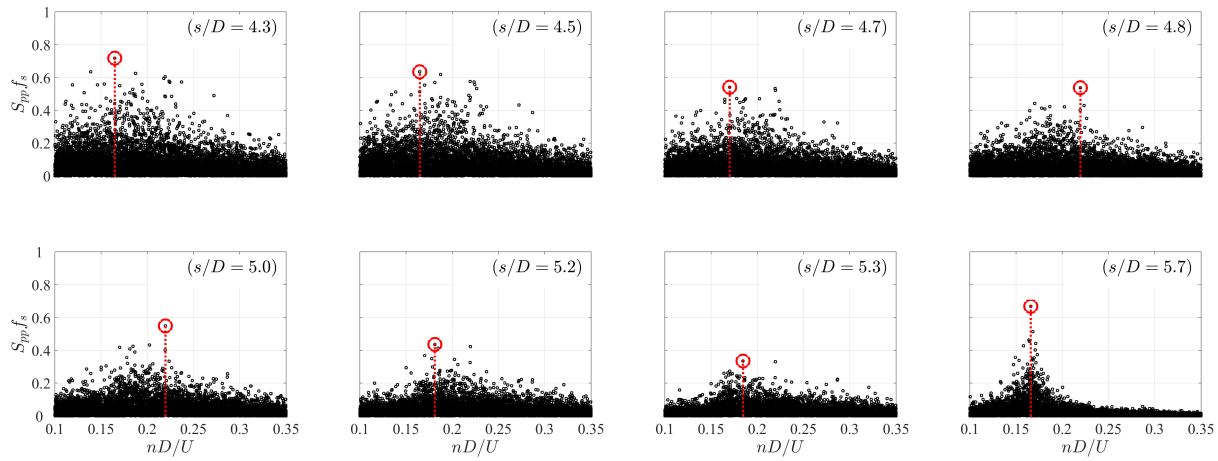

Figure 10. Magnitude of the fast Fourier transform of pressure records for some taps on the lateral side of the model (configuration #3, $I_u = 5.7\%$). The selected dominant peak reported in Figure 9 is highlighted.

Figure 11 shows the phase angle of the pressure coefficient fluctuations at the dominant frequency of vortex shedding, relative to that of the tap closer to the leading edge (tap 5 in Figure 2), along the lateral face of the cylinder. In smooth flow, the wavelength of pressure fluctuations is only slightly lower than the cross-section chord, that is just one vortex travels at a time along the cylinder surface. This means that the first mode of impinging shear-layer instability is active in the vortex shedding mechanism. This is in agreement with the numerical simulations reported in Mannini et al. (2010), Mannini et al. (2011) and with the measurements of Nakamura, Ohya, and Tsuruta (1991), who interestingly showed that the vortices become two for $B/D = 6$. Figure 11(a) also highlights that the phase angle is nearly null for $-2.5 \leq x/D \lesssim -1.5$, corresponding to the "pseudo-triangular region" clearly evidenced by the numerical simulations of Bruno, Fransos, et al. (2010). Then, a progressive phase shift of 360° can be detected in the range $-1.5 \lesssim x/D \lesssim 2$ and finally a nearly constant phase is observed again for $2 \lesssim x/D \leq 2.5$, well corresponding to the "mean reattached flow region" identified by Bruno and co-workers. These considerations allow estimating the mean convection velocity U_c of the main vortices forming in the pseudo-triangular region, travelling downstream along the lateral sides of the cylinder and finally shed in the wake. In fact, it is possible to write:

$$\frac{U_c}{U_\infty} = \frac{\lambda_s}{D} St \cong 0.4 \tag{1}$$

where U_∞ is the free-stream mean flow speed and $\lambda_s/D \cong 3.5$ is the normalized wavelength of the fluctuations at the vortex shedding frequency n_s and $St = 0.115$ is the previously mentioned Strouhal number. The result of Eq. (1) tells that the primary vortices travel along the lateral sides of the rectangular cylinder with a velocity much lower than the incoming flow speed. Nevertheless, Figure 11(a) clarifies that the velocity of the primary vortices tends to increase in the range $-2.5 \leq x/D \lesssim -0.33$, while it remains constant for $-0.33 \lesssim x/D \lesssim 2$, where the trend of phase angle is linear. It is to note that Bruno, Fransos, et al. (2010) obtained through a LES simulation $U_c/U_\infty = 0.48$ while Nakamura, Ohya, and Tsuruta (1991) estimated $U_c/U_\infty = 0.63$ for a rectangular 4:1 cylinder.

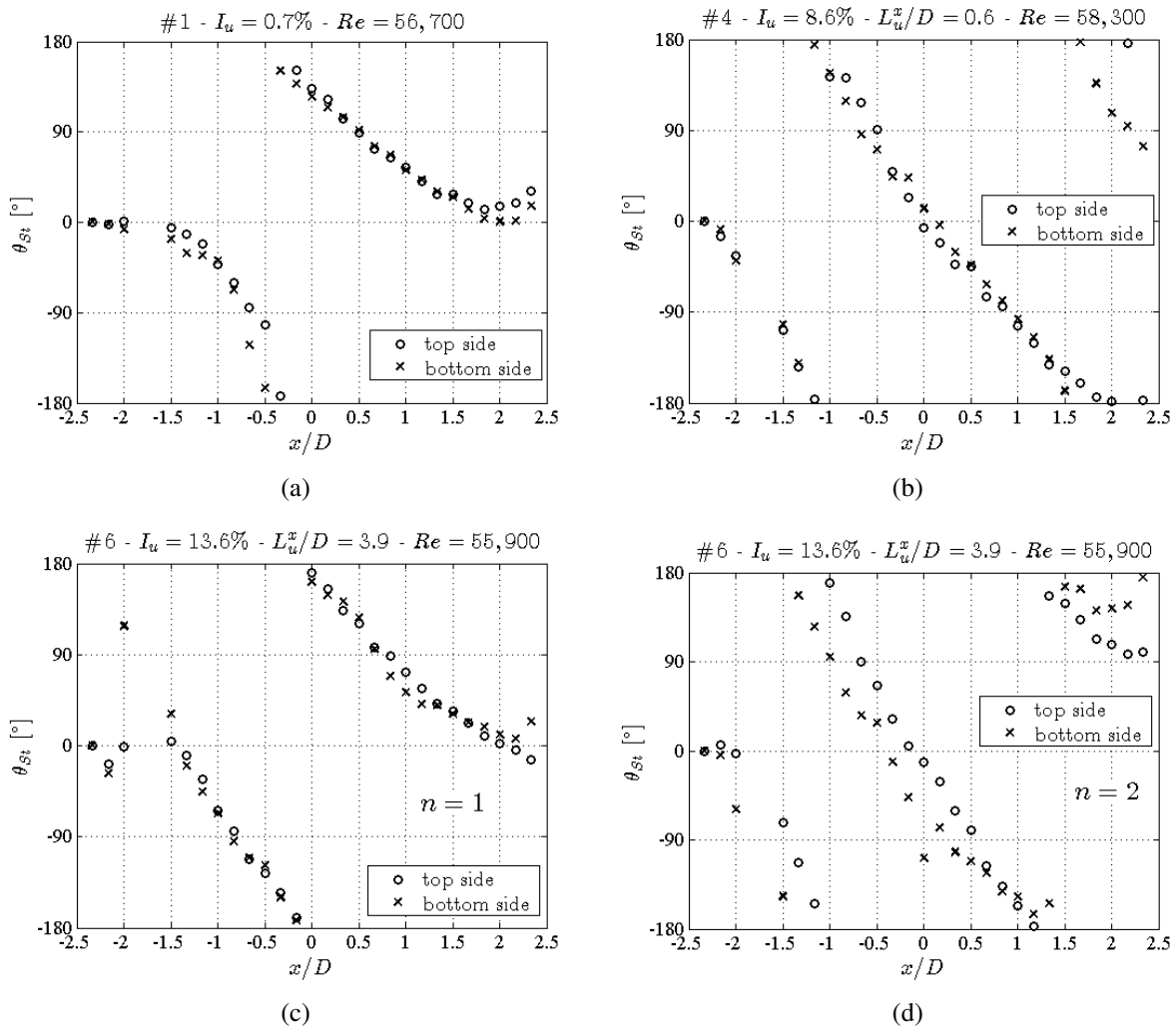

Figure 11. Phase angle of the fluctuating pressure coefficient component corresponding to the Strouhal frequency at different streamwise positions: (a) smooth flow ($St = 0.115$); (b) turbulent flow #4 ($St = 0.176$); (c) turbulent flow #6 ($n = 1$, $St = 0.121$); (d) turbulent flow #6 ($n = 2$, $St = 0.217$).

By contrast, Figure 11(b) clearly shows that, in a turbulent flow with $I_u = 8.6\%$ and $L_{ux}/D = 0.6$, the second mode of impinging shear-layer instability becomes dominant, as highlighted by the phase shift of 360° in about half chord of the model section. This means that two vortices travel at a time along each streamwise side of the cylinder, resulting in a significantly higher Strouhal number ($St = 0.176$). Interestingly, in a turbulent flow with higher intensity and larger integral length scale (configuration #6), the first and second modes of impinging shear-layer instability are found to coexist in the vortex shedding mechanism (Figures 11(c)-11(d)). It can be conjectured that this bi-modality is related to an intermittent behavior but further investigations are required to ascertain it.

5. CONCLUDING REMARKS

In this work, the aerodynamic behavior of the BARC rectangular 5:1 cylinder is studied in detail through pressure and wake measurements. The effect of incoming turbulence with various intensities and integral length scales was extensively studied. It was clearly shown that the length of the recirculation bubbles along the lateral sides of the cylinder significantly reduces due to the free-stream turbulence. In addition, turbulence significantly influences the vortex shedding mechanism of impinging shear-layer instability and is able to promote a switch from a dominant mode to another. This fact can also have important consequences on the flow-induced vibrations of flexible cylinders.

REFERENCES

Bartoli, G., Bruno, L., Buresti, G., Ricciardelli, F., Salvetti, M. V., and Zasso, A., 2008. *BARC overview document*. http://www.aniv-iawe.org/barc.

Bruno, L., Fransos, D., Coste, N., and Bosco, A., 2010. 3D flow around a rectangular cylinder: A computational study. Journal of Wind Engineering and Industrial Aerodynamics 98, 263–276.

Bruno, L., Salvetti, M. V., and Ricciardelli, F., 2014. Benchmark on the Aerodynamics of a Rectangular 5:1 Cylinder: An overview after the first four years of activity. Journal of Wind Engineering and Industrial Aerodynamics 126, 87–106.

Hourigan, K., Thompson, M. C., and Tan, B. T., 2001. Self-sustained oscillations in flows around long blunt plates. Journal of Fluids and Structures 15, 387–398.

Mannini, C., Marra, A. M., and Bartoli, G., 2014. VIV-galloping instability of rectangular cylinders: Review and new experiments. Journal of Wind Engineering and Industrial Aerodynamics 132, 109–124.

Mannini, C., Šoda, A., and Schewe, G., 2010. Unsteady RANS modelling of flow past a rectangular cylinder: Investigation of Reynolds number effects. Computers and Fluids 39, 1609–1624.

— 2011. Numerical investigation on the three-dimensional unsteady flow past a 5:1 rectangular cylinder. Journal of Wind Engineering and Industrial Aerodynamics 99, 469–482.

Marra, A. M., Mannini, C., and Bartoli, G., 2015. Measurements and improved model of vortex-induced vibration for an elongated rectangular cylinder. Journal of Wind Engineering and Industrial Aerodynamics 147, 358–367.

Matsumoto, M., 1996. Aerodynamic damping of prisms. Journal of Wind Engineering and Industrial Aerodynamics 59, 159–175.

Mills, R., Sheridan, J., and Hourigan, K., 2002. Response of base suction and vortex shedding from rectangular prisms to transverse forcing. Journal of Fluid Mechanics 461, 25–49.

Nakamura, Y., and Nakashima, M., 1986. Vortex excitation of prisms with elongated rectangular, H and ⊢ cross-sections. Journal of Fluid Mechanics 163, 149–169.

Nakamura, Y., and Ohya, Y., 1984. The effects of turbulence on the mean flow past two-dimensional rectangular cylinders. Journal of Fluid Mechanics 149, 255–273.

Nakamura, Y., Ohya, Y., and Tsuruta, H., 1991. Experiments on vortex shedding from flat plates with square leading and trailing edges. Journal of Fluid Mechanics 222, 437–447.

Naudascher, E., and Wang, Y., 1993. Flow-induced vibrations of prismatic bodies and grids of prisms. Journal of Fluids and Structures 7, 341–373.

Ohya, Y., Nakamura, Y., Ozono, S., Tsuruta, H., and Nakayama, R., 1992. A numerical study of vortex shedding from flat plates with square leading and trailing edges. Journal of Fluid Mechanics 236, 445–460.

Parkinson, G. V., 1965. Aeroelastic galloping in one degree of freedom. Proceedings of Wind Effects on Buildings and Structures: proceedings of the conference held at the National Physical Laboratory, Teddington, UK, Jun. 26-28, 1963. HMSO, London, 581–609.

Rockwell, D., and Naudascher, E., 1979. Self-sustained oscillations of impinging free shear layers. Annual Review of Fluid Mechanics 11, 67–94.

Shiraishi, N., and Matsumoto, M., 1983. On classification of vortex-induced oscillation and its application for bridge structures. Journal of Wind Engineering and Industrial Aerodynamics 14, 419–430.

Washizu, K., Ohya, A., Otsuki, Y., and Fujii, K., 1978. Aeroelastic instability of rectangular cyliders in a heaving mode. Journal of Sound and Vibration 59, 195–210.